[11] N. Mikami, M. Ebara, M. Yoshikawa, and M. Ohto, "Relationship between ultrasound-findings of low-echoic nodule of hepatic parenchyma in liver cirrhosis and development of hepatocellular carcinoma," *Nippon Shokakibyo Gakkai Zasshi*, Japan, vol. 87, pp. 1010–1019, 1990.
[12] H. Nakamura, T. Yahagi, S. Yoshino, M. Ohto, M. Ebara, and T. Kimura, "A method for pattern information of liver cirrhosis from ultrasonic image," *Trans. Inst. Electron., Inform., Communicat. Eng.*, vol. 2, pp. 316– 319, 1989.
[13] U. Raeth, D. Schlaps, B. Limberg, I. Zuna, A. Lorenz, D. Ing, G. Kaick, W. J. Lorenz, and B. Kommerell, "Diagnostic accuracy of computerized B-scan texture analysis and conventional ultrasonography in diffuse parenchymal and malignant liver disease," *J. Clin. Ultrasound*, vol. 13, pp. 87–99, 1985.
[14] J. M. Thijssen, B. J. Oosterveld, P. C. Hartman, and G. J. E. Rosenbusch, "Correlations between acoustic and texture parameters from RF and B-mode liver echograms," *Ultrasound Med. Biol.*, vol. 19, pp. 13–20, 1993.
[15] J. S. DaPonte and P. Sherman, "Classification of ultrasonic image texture by statistical discriminant analysis and neural networks," *Comput. Med. Imag. Graph.*, vol. 15, pp. 3–9, 1991.
[16] M. S. Gebbinck, J. M. Thijssen, and T. E. Schouten, "Application of neural networks for the classification of diffuse liver disease by quantitative echography," *Ultrasonic Imag.*, vol. 15, pp. 205– 217, 1993.
[17] Y. M. Kadah, A. A. Frag, J. M. Zurada, A. M. Badawi, and A. M. Youssef, "Classification algorithms for quantitative tissue characterization of diffuse liver disease from ultrasound images," *IEEE Trans. Med. Imag.*, vol. 15, pp. 466–478, 1996.
[18] H. Sujana, S. Swarnamani, and S. Suresh, "Application of artificial neural networks for the classification of liver lesions by image texture parameters," *Ultrasound Med., Biol.*, vol. 22, no. 9, pp. 1777–1181, 1996.

A Parametric Fitting Algorithm for Segmentation of Cell Images

Hai-Shan Wu, Joseph Barba,* and Joan Gil

***Abstract*— This paper presents a parametric fitting algorithm for segmentation of cervical and breast cell images from cytology smears. A parametric elliptical model for cells is introduced and the parameters adjusted to fit the cell shapes while minimizing a cost function. Segmentation results of noisy human cervical cell and textured breast cell images demonstrate that the proposed parametric fitting algorithm is very successful in segmentation of images of both nonoverlapped and overlapped elliptically shaped cells.**

***Index Terms*—Biomedical image processing, cell images, image segmentation, quantitative pathology.**

I. Introduction

Pathologists usually make diagnostic decisions by viewing specimen cells and assessing their various diagnostically important parameters and patterns such as size, shapes, and textures [1]. Accurate measurements of the cell parameters with a computer-aided image processing system is useful in quantitative pathology and medicine [2]–[4]. To obtain these critical parameters accurate segmentation of the nuclear regions is required.

Manuscript received May 9, 1996; revised May 9, 1997. *Asterisk indicates corresponding author.*

H.-S. Wu and J. Gil are with the Department of Pathology, Mount Sinai School of Medicine, New York, NY 10029 USA.

*J. Barba is with the Department of Electrical Engineering, City College of New York, 140th Street and Convent Avenue, New York, NY 10031 USA (e-mail: barba@ee-mail.engr.ccny.cuny.edu).

Publisher Item Identifier S 0018-9294(98)01615-2.

From an application point of view, image segmentation techniques can be categorized as interactive (semiautomatic) and noninteractive (automatic). Interactive approaches usually provide reliable segmentation results but require the participation of a user in the image segmentation process [5]. Automatic image-segmentation methods are usually nonparametric and generally based on local image information such as regions, edges, histograms, or clusters. Edge-based or gradient-based segmentation methods rely on the idea of discontinuity of image intensities or texture at the boundary between different objects [6]–[8]. Histogram-based and unsupervised clustering algorithms for image segmentation are successful for those images with uniform illumination or other mapped discrimination features [9], [10]. Region-based algorithms [11]–[13] employ region growing, region splitting and merging to separate different objects with homogeneous intensities. The edge-based methods and clustering approaches are generically sensitive to image noise and artifacts. The region-based algorithms, which are less sensitive to image noise, are usually computationally more expensive.

There have been many nonparametric algorithms reported in the literature for the segmentation of images [6]–[17], however, little has been done with regards to parametric modeling segmentation approaches incorporating *a priori* knowledge of the objects to be identified. Segmentation performance can be greatly improved by incorporating *a priori* knowledge about the specific type of images being segmented. The Hough transform is a parametric method useful for shape analysis [18], [19]. After edges are detected, the Hough transform is performed to detect a desired shape. The objects are then located by searching for the peaks in the parametric space. Although Hough transforms are successful in detection of analytic patterns, such as lines, circles, and ellipses, there are several shortcomings with this technique when used for segmentation of real images. Besides the excessive storage requirements and computational complexity, image textures, and noise usually degrade edge detection making it difficult to find the correct peaks in the parameter space. Since it is an edge-based method, it is sensitive to image noise and textures. To improve the segmentation performance of real images that are generally textured and noisy we incorporate the *a priori* knowledge of the cell shapes and also make use of information from interior of regions instead of their boundaries. In this paper, we introduce a parametric segmentation algorithm for human breast and cervical cell images obtained from a light microscope by optimally fitting generic shapes. The cells can then be segmented from the fitting functions determined by their parameters.

This correspondence is organized as follows. Section II introduces the parametric elliptical waveform functions used to describe the local region of a cell image. Section III presents an elliptical waveform fitting algorithm to approximate a real single cell image with the proposed parametric ellipse-like function. The algorithm involves a coarse optimization search followed by a fine optimization procedure which provide the optimal solutions for the parameters. Section IV discusses the computational complexities of the proposed algorithm. Section V describes the application of the proposed algorithm for segmentation of images with overlapped cells. Section VI provides the experimental results of the algorithm for cell images. Comparisons of the simulation performance are also provided. Brief conclusions are given in Section VII.

II. Human Cervical and Breast Cell Image Model

The human cervical cells as seen in cytology smears usually have ellipse-like shaped boundaries as shown in the light microscope

images in Fig. 1(a). The darker region of the image indicates the cell nucleus and the brighter areas correspond to the background which includes the cytoplasm and empty regions. To extract clinical data from the cell image requires segmenting the cell nuclear regions from the background. Region profiles can be defined as the boundary which separates regions whose pixels have significantly different properties. Let the characteristic function of an image containing only one complete cervical cell be defined as $P(n_1, n_2) = 1$ for $(n_1, n_2) \in R_c$; 0 otherwise, where (n_1, n_2) denotes the discrete coordinate and R_c is the region of the cell. $P(n_1, n_2)$ equals one if the pixel at the coordinate (n_1, n_2) belongs to the cell region, zero otherwise. Suppose that an ideal cervical cell image can be modeled as $\tilde{f}(n_1, n_2) = A_1 P(n_1, n_2) + A_2[1 - P(n_1, n_2)]$, a two-level nuclear image with value A_1 inside the cell and A_2 outside. The idealized cervical cell image $\tilde{f}(n_1, n_2)$ usually has a well defined elliptical shape which can be described mathematically. To improve the segmentation of the cell image the *a priori* knowledge of the cervical cell shape should be incorporated. Then the image segmentation problem is converted to a parametric optimization problem where the parameters are determined based on the given image information. After the parameters of the mathematical model are determined the cell image can be reconstructed based solely on these parameters and the segmentation of the image is obtained from the reconstructed cell image.

To make use of the elliptical shape as the *a priori* knowledge, we compose a gray level image incorporating the shape information to approximate the desired image model. The elliptical shape can be described by a vector of five coefficients which must be included in the parametric representation. We compose a function whose value is low inside the elliptical boundaries and high outside. The elliptical boundaries can then be extracted simply by applying a thresholding procedure to the composed function. If the parameters c_4 and c_5 are both positive, we observe

$$[(n_1 + c_2)\cos(c_6) - (n_2 + c_3)\sin(c_6)]^2 + c_5[(n_1 + c_2)\sin(c_6) + (n_2 + c_3)\cos(c_6)]^2 = c_4 \quad (1)$$

denotes an elliptical curve in the (n_1, n_2) domain, where c_5 is the squared ratio of the two axes of the ellipse, c_4 along with c_5 defines the size of the ellipse, c_2 and c_3 determine the center of the ellipse, and c_6 indicates the orientation of the ellipse. We define the function

$$g_{\mathbf{c}}(n_1, n_2) = [(n_1 + c_2)\cos(c_6) - (n_2 + c_3)\sin(c_6)]^2 + c_5[(n_1 + c_2)\sin(c_6) + (n_2 + c_3)\cos(c_6)]^2 - c_4. \quad (2)$$

If the constant $\Lambda > -c_4$, the equation $g_{\mathbf{c}}(n_1, n_2) = \Lambda$ will represent an elliptical curve. With the value Λ increasing from $-c_4$ to $+\infty$, the ellipse grows monotonically from as small as a dot to an infinite large one. If $g_{\mathbf{c}}(n_1, n_2) = 0$ corresponds to the cell contour, $g_{\mathbf{c}}(n_1, n_2) < 0$ will be the cell region and $g_{\mathbf{c}}(n_1, n_2) > 0$ the region outside of the cell contour. This can be described by a sign function with $g_{\mathbf{c}}(n_1, n_2)$ as the input. However, to maintain a differentiable parametric function, we use the antisymmetric arc tangent function instead. Adding the scale and mean, the fitting parametric function is then defined by

$$\hat{f}_{\mathbf{c}}(n_1, n_2) = c_0 \tan^{-1}[A g_{\mathbf{c}}(n_1, n_2)] + c_1 \quad (3)$$

where $\hat{f}_{\mathbf{c}}(n_1, n_2)$ is a function of the seven-coefficient parameter vector, $\mathbf{c} = (c_0, c_1, \cdots, c_6)^t$, and the value A. For a given value A, the vector $\mathbf{c}$ determines the waveform $\hat{f}_{\mathbf{c}}(n_1, n_2)$. If $A \to \infty$, $\hat{f}_{\mathbf{c}}(n_1, n_2)$ approaches the ideal two-level cell image $\tilde{f}(n_1, n_2)$ whose two levels are $c_1 + (\pi/2)c_0$ and $c_1 - (\pi/2)c_0$, respectively.

The breast cells that are usually highly textured appear different from the cervical cells which are more homogeneous in the cell regions. However, as recognized by pathologists, like cervical cells, a breast cell also has an elliptical shape and its average intensity is relatively lower than its surrounding background. Thus, the above model is appropriate for approximating both breast and cervical cells.

III. Waveform Fitting

To find the global optimal fitting a coarse optimization search is first employed and followed by a fine optimization procedure. The coarse optimization is used to find a rough solution near the global optimum solution thereby preventing the subsequent fine optimization procedure from being trapped in a local optimal state. The fine optimization procedure refines the solution in a local region by minimizing the cost function that measures the fit of the approximation function.

Assume that the digital image $f(n_1, n_2)$ is of size $N_1 \times N_2$ and contains only one cell. Let the cost function, $\Xi(\mathbf{c})$, be defined as the mean-square error (MSE) of the approximation by the above parametric function

$$\Xi(\mathbf{c}) = \frac{1}{N_1 N_2} \sum_{n_1=0}^{N_1-1} \sum_{n_2=0}^{N_2-1} [\hat{f}_{\mathbf{c}}(n_1, n_2) - f(n_1, n_2)]^2. \quad (4)$$

Thus, the cell segmentation problem transforms to finding the vector $\mathbf{c}$ such that the cost function, $\Xi(\mathbf{c})$, is minimized.

A. Coarse Optimization Search

Although there are many available optimization methods they usually converge to local optimal solutions and their performance depends on the initial state. It is more likely to converge to the global optimal solution if the initial vector is close to the global optimum since there is less likelihood of being trapped in a local minimum. Suppose that the cost function is relatively smooth. If the cost function is sampled with a rather small sampling period it is very likely that the neighborhood about the global optimum will be sampled at least once. Thus, the initial procedure is to find a sample which is in the neighborhood of the global optimum. As expected, the sample we are seeking should yield a lower cost than other samples since it is closer to the global optimum. Sampling the seven-dimensional parameter space of the vector $\mathbf{c}$ with a small sampling period produces large amount of data making an exhaustive search very expensive. There are two ways to reduce the computational complexity. The first is to restrict the searching range by using available *a priori* information to form an initial guess of the seven-dimensional vector, $\overline{\mathbf{c}} = (\overline{c}_0, \overline{c}_1, \cdots, \overline{c}_6)^t$. The other is to sample and search in one dimension at one time; the seven dimensions are processed in turn iteratively. Let $\text{Min}(f)$ and $\text{Max}(f)$ represent the minimum and maximum intensities of the image $f(n_1, n_2)$, respectively. For the cervical and breast cell images from cytology smears a cell usually has lower average intensity than its neighboring background. Therefore, $\text{Min}(f)$ is expected to be the intensity of a cell pixel while $\text{Max}(f)$ is the intensity of a background pixel. We let $\overline{c}_1 - (\pi/2)\overline{c}_0 = \text{Min}(f)$ and $\overline{c}_1 + (\pi/2)\overline{c}_0 = \text{Max}(f)$. Thus, the values of $\overline{c}_0$ and $\overline{c}_1$ can be determined from the above two equations. The coefficients c_2 and c_3 correspond to the coordinate of the ellipse center which can be approximated by filtering the image with a very narrow band lowpass finite impulse response (FIR) linear filter. The ellipse center corresponds to the image element with the minimum intensity. The coefficient c_4 corresponds to the size of the cell. If the cell is round, then c_4 is the squared radius of the circular cell contour. Cervical cell size varies but lies in a known limited range. The coefficient $\overline{c}_4$ can be initially chosen as the middle range value. The positive coefficient c_5 is the squared ratio of the two axes of the elliptical cell profile. When c_5 is larger than one, it is the squared ratio of the major axis

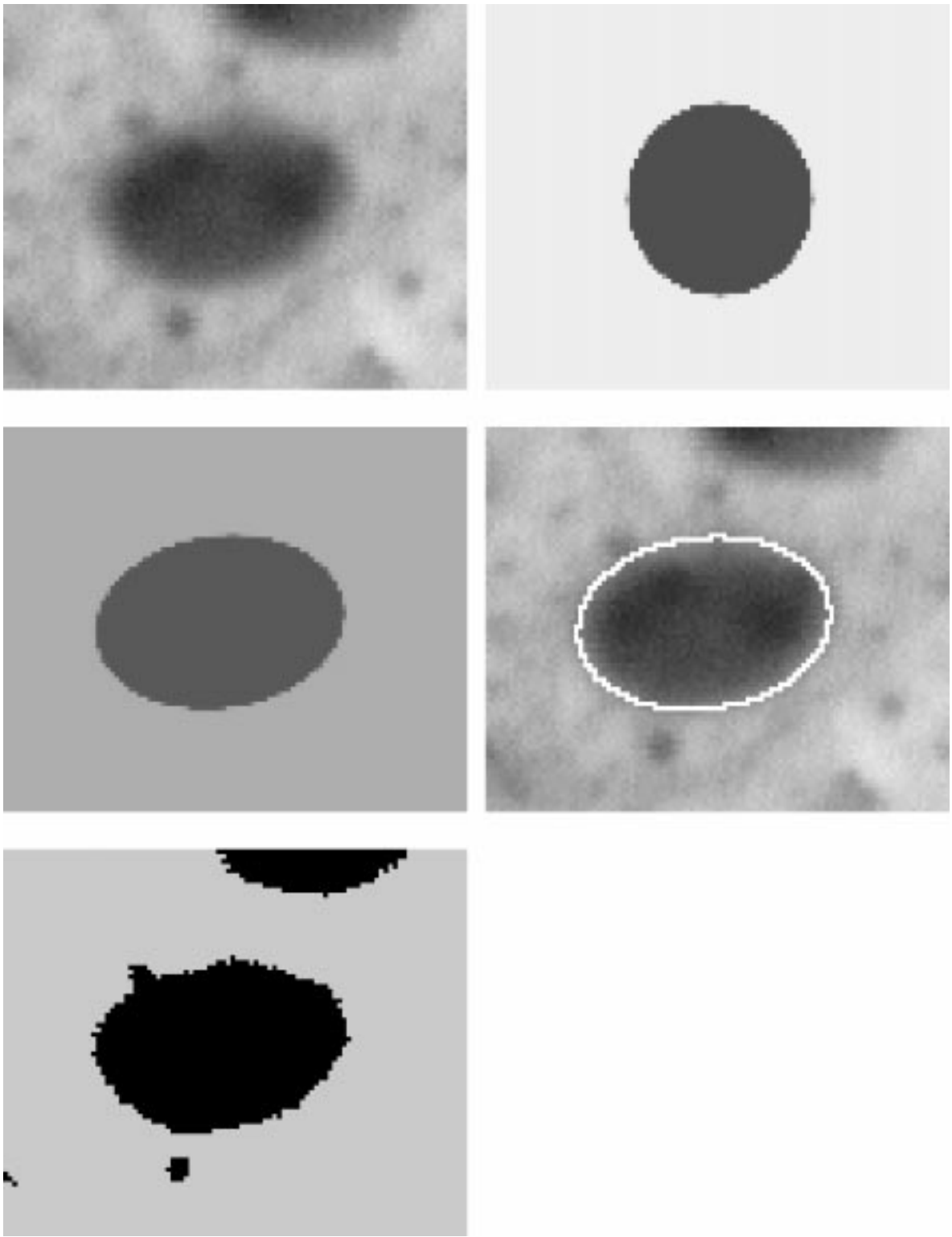

Fig. 1. Parametric segmentation for a single cell image. (a) The original cell image, (b) initial fitting parametric image, (c) final fitting parametric image, (d) the original cell image superimposed with the extracted cell contour from (d), and (e) segmentation map of the K-means clustering method.

to the minor axis, otherwise, it is the squared ratio of the minor axis to the major axis. We initially set $\overline{c}_5 = 1$ to start with a circular cell profile. The orientation of the elliptical cell is represented by the last coefficient c_6 which can be considered a random variable uniformly distributed in $[-\pi, \pi]$. When $\overline{c}_5 = 1$, the value of $\overline{c}_6$ does not affect the cost function and we simply set it to zero at the beginning.

After selecting the coefficients in the above manner the vector $\overline{\mathbf{c}}$ can still be very far from the desired value. Prior to using a fine optimization method a coarse search is conducted to find an initial state which is close to the desired global optimal state. Let the range of coefficient c_i be $[\theta_-(i), \theta_+(i)]$ and the sampling period of the coefficient c_i be $\Delta_i = r_i/L$, where the maximum number of sample

is $2L+1$, r_i is the searching distance and the supposed searching range is $[\bar{c}_i - r_i, \bar{c}_i + r_i]$. Since some natural restrictions apply, the actual searching range $[\Theta_-(i), \Theta_+(i)]$ is usually smaller than the supposed range so that $[\Theta_-(i), \Theta_+(i)] = [\max(\theta_-(i), \bar{c}_i - r_i), \min(\theta_+(i), \bar{c}_i + r_i)]$. Based on the natural characteristics of the parameters, the restrictions include $0 < c_0 < 255$, $0 < c_1 < 255$, $0 < -c_2 < N_1$, $0 < -c_3 < N_2$, $0 < c_4$, and $0 < c_5$. Thus, $\theta_-(i) = 0$, for $i = 0, 1, \cdots, 5$, $\theta_+(0) = 255$, $\theta_+(1) = 255$, $\theta_+(2) = N_1 - 1$, $\theta_+(3) = N_2 - 1$, and the rest are ∞ for $\theta_+(i)$ and $-\infty$ for $\theta_-(i)$, respectively.

The coarse optimization procedure can be summarized as follows. Let

1) $\bar{c}_i^{(0)} = \bar{c}_i$, for $i = 0, 1, \cdots, 6$. Specify the integer L, which is half the number of samples taken in each coefficient axis, the value of r_i, for $i = 0, 1, \cdots, 6$, which restrict the range of the search for each coefficient, and a small positive value δ which is used as a threshold to terminate the procedure. Set $i = 0$ and $k = 0$.
2) Let
$$j = \arg\min_l \Xi\left[\bar{c}_0^{(k+1)}, \cdots, \bar{c}_{i-1}^{(k+1)}, \bar{c}_i^{(k)} + l\Delta_i, \cdots, \bar{c}_6^{(k)}\right], \quad \text{for } l = L_-(i), \cdots, 0, 1, \cdots, L_+(i) \tag{5}$$
where $L_-(i) = [\Theta_-(i) - \bar{c}_i^{(k)}]/\Delta_i$ and $L_+(i) = [\Theta_+(i) - \bar{c}_i^{(k)}]/\Delta_i$. Adjust the ith coefficient: $\bar{c}_i^{(k+1)} = \bar{c}_l^{(k)} + j\Delta_i$.
3) If $i < 7$, let $i = i + 1$ and go back to Step 2), otherwise, evaluate $\Xi[\bar{\mathbf{c}}^{(k)}] - \Xi[\bar{\mathbf{c}}^{(k+1)}]$, the reduction of the cost during the current iteration. If this cost reduction is larger than δ, set $i = 0$ and go to Step 2) for the next iteration; otherwise terminate the procedure and output the vector of coefficients $\bar{\mathbf{c}}^{(k+1)}$ as the initial approximation to the global optimal state.

B. Fine Optimization

The coarse search is expected to produce a coefficient vector, $\bar{\mathbf{c}}^{(k+1)}$, which is close to the global optima. Let the coefficient vector obtained be the initial state, $\mathbf{c}^{(0)} = \bar{\mathbf{c}}^{(k+1)}$, of the iterative fine optimization procedure. The parameter vector is iteratively adjusted as

$$\mathbf{c}^{(k+1)} = \mathbf{c}^{(k)} - \eta\Delta\mathbf{c}^{(k)} \tag{6}$$

where the integer k is the iteration index, η is a small adjustment constant and the seven-dimensional vector $\Delta\mathbf{c}^k = (\Delta c_0^k \Delta c_1^k \cdots \Delta c_6^k)^t$ with

$$\Delta c_0^{(k)} = \frac{1}{N_1N_2}\sum_{n_1=0}^{N_1-1}\sum_{n_2=0}^{N_2-1} \tan^{-1} \cdot [Ag_{\mathbf{c}^{(k)}}(n_1, n_2)][\hat{f}_{\mathbf{c}^k}(n_1, n_2) - f(n_1, n_2)] \tag{7}$$

$$\Delta c_1^{(k)} = \frac{1}{N_1N_2}\sum_{n_1=0}^{N_1-1}\sum_{n_2=0}^{N_2-1} [\hat{f}_{\mathbf{c}^k}(n_1, n_2] - f(n_1, n_2)] \tag{8}$$

$$\Delta c_2^{(k)} = \frac{1}{N_1N_2}\sum_{n_1=0}^{N_1-1}\sum_{n_2=0}^{N_2-1} \frac{2A\, c_0^{(k)}}{1 + [Ag_{\mathbf{c}^{(k)}}(n_1, n_2)]^2} \cdot \left(\left\{\left(n_1 + c_2^{(k)}\right)\cos\left[c_6^{(k)}\right] - \left(n_2 + c_3^{(k)}\right)\sin\left[c_6^{(k)}\right]\right\} \cdot \cos\left[c_6^{(k)}\right] + c_5^{(k)}\left[\left(n_1 + c_2^{(k)}\right)\sin\left(c_6^{(k)}\right) + \left(n_2 + c_3^{(k)}\right) \cdot \cos\left(c_6^{(k)}\right)\right]\sin\left[c_6^{(k)}\right]\right) \cdot \left[\hat{f}_{\mathbf{c}^k}(n_1, n_2) - f(n_1, n_2)\right] \tag{9}$$

$$\Delta c_3^{(k)} = \frac{1}{N_1N_2}\sum_{n_1=0}^{N_1-1}\sum_{n_2=0}^{N_2-1} \frac{2Ac_0^{(k)}}{1 + [Ag_{\mathbf{c}^{(k)}}(n_1, n_2)]^2} \cdot \left(\left\{\left(n_1 + c_2^{(k)}\right)\cos\left[c_6^{(k)}\right] - \left(n_2 + c_3^{(k)}\right)\sin\left[c_6^{(k)}\right]\right\} \cdot \left\{-\sin\left[c_6^{(k)}\right]\right\} + c_5^{(k)} \cdot \left[\left(n_1 + c_2^{(k)}\right)\sin\left(c_6^{(k)}\right) + \left(n_2 + c_3^{(k)}\right)\cos\left(c_6^{(k)}\right)\right] \cdot \cos\left[c_6^{(k)}\right]\right)\left[\hat{f}_{\mathbf{c}^k}(n_1, n_2) - f(n_1, n_2)\right] \tag{10}$$

$$\Delta c_4^{(k)} = \frac{1}{N_1N_2}\sum_{n_1=0}^{N_1-1}\sum_{n_2=0}^{N_2-1} \frac{-Ac_0^{(k)}}{1 + [Ag_{\mathbf{c}^{(k)}}(n_1, n_2)]^2} \cdot \left[\hat{f}_{\mathbf{c}^k}(n_1, n_2) - f(n_1, n_2)\right] \tag{11}$$

$$\Delta c_5^{(k)} = \frac{1}{N_1N_2}\sum_{n_1=0}^{N_1-1}\sum_{n_2=0}^{N_2-1} \cdot \frac{Ac_0^{(k)}\left[\left(n_1 + c_2^{(k)}\right)\sin\left(c_6^{(k)}\right) + \left(n_2 + c_3^{(k)}\right)\cos\left(c_6^{(k)}\right)\right]^2}{1 + [Ag_{\mathbf{c}^{(k)}}(n_1, n_2)]^2} \cdot \left[\hat{f}_{\mathbf{c}^k}(n_1, n_2) - f(n_1, n_2)\right] \tag{12}$$

$$\Delta c_6^{(k)} = \frac{1}{N_1N_2}\sum_{n_1=0}^{N_1-1}\sum_{n_2=0}^{N_2-1} \frac{2Ac_0^{(k)}}{1 + [Ag_{\mathbf{c}^{(k)}}(n_1, n_2)]^2} \cdot \left\{\left[\left(n_1 + c_2^{(k)}\right)\cos\left(c_6^{(k)}\right) - \left(n_2 + c_3^{(k)}\right)\sin\left(c_6^{(k)}\right)\right] \cdot \left[-\left(n_1 + c_2^{(k)}\right)\sin\left(c_6^{(k)}\right) - \left(n_2 + c_3^{(k)}\right)\cos\left(c_6^{(k)}\right)\right] + c_5^{(k)}\left[\left(n_1 + c_2^{(k)}\right)\sin\left(c_6^{(k)}\right) + \left(n_2 + c_3^{(k)}\right) \cdot \cos\left(c_6^{(k)}\right)\right]^2 \cdot \left[\left(n_1 + c_2^{(k)}\right)\cos\left(c_6^{(k)}\right) - \left(n_2 + c_3^{(k)}\right)\sin\left(c_6^{(k)}\right)\right]^2\right\} \cdot \left[\hat{f}_{\mathbf{c}^k}(n_1, n_2) - f(n_1, n_2)\right]. \tag{13}$$

The iterative procedure stops when the magnitude of the adjustment, $\|\eta\Delta\mathbf{c}^{(k)}\|$, is small enough and the resulting vector $\mathbf{c} = \mathbf{c}^{(k+1)}$ is assumed to be the best solution.

The cell region is recognized as the ellipse shaped region described by

$$R_c = \{(n_1, n_2) | [(n_1 + c_2)\cos(c_6) - (n_2 + c_3)\sin(c_6)]^2 + c_5[(n_1 + c_2)\sin(c_6) + (n_2 + c_3)\cos(c_6)]^2 \le c_4. \tag{14}$$

Because it was assumed that the image contains only one cell, the rest of the image is background. If the image contains more than one cells, the above procedure can be applied with slight modification.

IV. Computational Complexity

The segmentation procedure consists of a coarse search to provide good initial state and a subsequent fine optimization. Even by restricting the search region in the seven-dimensional parameter space by incorporating *a priori* information the search is computationally demanding. If each variable is sampled $2L+1$ times the total number of samples will be $7^{(2L+1)}$. To simplify the computation the search is performed serially instead of attempting an exhaustive search for the parameters. Each serial iteration processes only $7(2L+1)$ samples. Although the serial search needs repeated iterations it is simple in each step and the iterative procedure converges quickly, usually in less than a few dozens iterations.

The fine optimization is an iterative procedure involving additions and multiplications of sinusoidal terms. The repeated use of the sinusoidal functions is facilitated by evaluating and storing the values for reuse. If the subimage is of size of $N_1 \times N_2$, there are $N_1 N_2$ computations of arctangent in each iteration. Terms such as $(n_1 + c_2^{(k)})$, $(n_2 + c_3^{(k)})$, $2Ac_0^{(k)}/\{1 + [Ag_{\mathbf{c}^{(k)}}(n_1, n_2)]^2\}$, $\{(n_1 + c_2^{(k)}) \cos[c_6^{(k)}] - (n_2 + c_3^{(k)}) \sin(c_6^{(k)}]\}$, and $c_5^{(k)}[(n_1 + c_2^{(k)}) \sin(c_6^{(k)}) + (n_2 + c_3^{(k)}) \cos(c_6^{(k)})]$, are evaluated once and reused in each iteration. This results in $24N_1N_2$ multiplications in each iteration where a division is counted as one multiplication in complexity. Since the initial state is already close to the global optimal state it is expected to converge quickly. In addition, the small subimage size also simplifies the computation.

V. Segmentation of Overlapped Cells

The algorithm for segmentation of isolated cells can be extended to the segmentation of overlapped cells after some necessary modifications. In this section, we discuss the segmentation of two overlapped cells. The algorithm can be extended to multiple overlapped cells in a similar manner. The parametric function of two cells is revised from that of single cell in (3) to

$$\hat{f}_{(\mathbf{c},\,\mathbf{c}')}(n_1,\,n_2) = c_0 \tan^{-1}\{A \min[g_{\mathbf{c}}(n_1,\,n_2),\, g_{\mathbf{c}'}(n_1,\,n_2)]\} + c_1 \tag{15}$$

where

$$g_{\mathbf{c}}(n_1, n_2) = [(n_1 + c_2)\cos(c_6) - (n_2 + c_3)\sin(c_6)]^2 + c_5[(n_1 + c_2)\sin(c_6) + (n_2 + c_3)\cos(c_6)]^2 - c_4 \tag{16}$$

and

$$g_{\mathbf{c}'}(n_1,\,n_2) = \left[(n_1 + c_2')\cos(c_6') - (n_2 + c_3')\sin(c_6')\right]^2 + c_5'\left[(n_1 + c_2')\sin(c_6') + (n_2 + c_3')\cos(c_6')\right]^2 - c_4'. \tag{17}$$

The cost function of (4) is modified to

$$\Xi(\mathbf{c},\,\mathbf{c}') = \frac{1}{N_1N_2}\sum_{n_1=0}^{N_1-1}\sum_{n_2=0}^{N_2-1}\big(c_0 \tan^{-1} \cdot \{A \min[g_{\mathbf{c}}(n_1,\,n_2),\, g_{\mathbf{c}'}(n_1,\,n_2)]\} + c_1 - f(n_1,\,n_2)\big)^2. \tag{18}$$

The coarse search procedure will use the modified cost function (18) to search for 12 coefficients, c_i, for $i = 0,\,1,\,\cdots,\,6$, and c_i', for $i = 2,\,3,\,\cdots,\,6$, for the approximately optimal solution followed by a fine optimization which iteratively adjust the coefficients by

$$c_i^{(k+1)} = c_i^{(k)} - \eta \Delta c_i^{(k)}, \qquad \text{for } i = 0,\,1,\,\cdots,\,6 \tag{19}$$

and

$$c_i'^{(k+1)} = c_i'^{(k)} - \eta \Delta c_i'^{(k)}, \qquad \text{for } i = 2,\,3,\,\cdots,\,6 \tag{20}$$

with adjustments as follows:

$$\Delta c_0^{(k)} = \frac{1}{N_1N_2}\sum_{n_1=0}^{N_1-1}\sum_{n_2=0}^{N_2-1} \cdot \{\hat{f}_{[\mathbf{c}^{(k)},\,\mathbf{c}'^{(k)}]}(n_1,\,n_2) - f(n_1,\,n_2)\} \cdot \tan^{-1}\{A \min[g_{\mathbf{c}^{(k)}}(n_1,\,n_2),\, g_{\mathbf{c}'^{(k)}}(n_1,\,n_2)]\} \tag{21}$$

$$\Delta c_1^{(k)} = \frac{1}{N_1N_2}\sum_{n_1=0}^{N_1-1}\sum_{n_2=0}^{N_2-1} \cdot \left\{\hat{f}_{[\mathbf{c}^{(k)},\,\mathbf{c}'^{(k)}]}(n_1,\,n_2) - f(n_1,\,n_2)\right\} \tag{22}$$

$$\Delta c_i^{(k)} = \frac{1}{N_1N_2}\sum_{n_1=0}^{N_1-1}\sum_{n_2=0}^{N_2-1} \left\{\hat{f}_{[\mathbf{c}^{(k)},\,\mathbf{c}'^{(k)}]}(n_1,\,n_2) - f(n_1,\,n_2)\right\} \cdot \frac{Ac_0^{(k)}\,u[g_{\mathbf{c}^{(k)}}(n_1,\,n_2) - g_{\mathbf{c}'^{(k)}}(n_1,\,n_2)]}{1 + \{A \min[g_{\mathbf{c}^{(k)}}(n_1,\,n_2),\, g_{\mathbf{c}'^{(k)}}(n_1,\,n_2)]\}^2} \cdot \frac{\partial g_{\mathbf{c}^{(k)}}(n_1,\,n_2)}{\partial c_i}, \qquad \text{for } i = 2,\,3,\,\cdots,\,6 \tag{23}$$

and

$$\Delta c_i'^{(k)} = \frac{1}{N_1N_2}\sum_{n_1=0}^{N_1-1}\sum_{n_2=0}^{N_2-1} \cdot \left\{\hat{f}_{[\mathbf{c}^{(k)},\,\mathbf{c}'^{(k)}]}(n_1,\,n_2) - f(n_1,\,n_2)\right\} \cdot \frac{Ac_0^{(k)}\{1 - u[g_{\mathbf{c}^{(k)}}(n_1,\,n_2) - g_{\mathbf{c}'^{(k)}}(n_1,\,n_2)]\}}{1 + \{A \min[g_{\mathbf{c}^{(k)}}(n_1,\,n_2),\, g_{\mathbf{c}'^{(k)}}(n_1,\,n_2)]\}^2} \cdot \frac{\partial g_{\mathbf{c}'^{(k)}}(n_1,\,n_2)}{\partial c_i'}, \qquad \text{for } i = 2,\,3,\,\cdots,\,6 \tag{24}$$

where the derivatives $[\partial g_{\mathbf{c}^{(k)}}(n_1,\,n_2)]/\partial c_i$ and $\partial g_{\mathbf{c}'^{(k)}}(n_1,\,n_2)/\partial c_i'$, for $i = 2,\,3,\,\cdots,\,6$, can be acquired from (16) and (17), and $u(\tau)$ is the step function which equals one if $\tau \geq 0$, zero otherwise.

The above procedure produces vectors of the parameters $\mathbf{c}$ and $\mathbf{c}'$ from which the two cell regions can be extracted as $\{(n_1,\,n_2)|g_{\mathbf{c}}(n_1,\,n_2) \leq 0\}$ and $\{(n_1,\,n_2)|g_{\mathbf{c}'}(n_1,\,n_2) \leq 0\}$, respectively.

VI. Experimental Results

Fig. 1(a) shows a gray-level cervical image of size $N_1 \times N_2 = 80 \times 100$ taken by a light microscope at projection 60 ×, sampled at the resolution of 4.4 samples per micron, and quantized into 256 levels. The cervical cell specimen was stained by the Crocker and Nar staining technique. The image contains a single elliptical shaped cervical cell in a rather noisy background. To reduce the image noise and the annoying artifacts we apply a preprocessing Gaussian lowpass filter with truncated Gaussian impulse response $A_g \exp[(-n_1^2 + n_2^2)/2\sigma_g^2]$, for $|n_1| \leq N_{g_1}$ and $|n_2| \leq N_{g_2}$, zero otherwise, where A_g is the normalization factor, N_{g_1} and N_{g_2} specify the region of support, and σ_g^2 determine the bandwidth of the filter. The filter with parameters $N_{g_1} = N_{g_2} = 5$ and $\sigma_g^2 = 5.0$ is used. It starts with $\hat{f}_{\overline{\mathbf{c}}^{(0)}}(n_1,\,n_2)$ in which the parameter vector, $\overline{\mathbf{c}}^{(0)}$, is estimated from the filtered cell image. $\overline{c}^{(0)}(1)$ is selected as the average level of the image given by $\overline{c}^{(0)}(1) = N_1N_2/[\sum_{n1=0}^{N_1-1}\sum_{n2=0}^{N_2-1} f(n_1,\,n_2)] = 114.7$. $\overline{c}^{(0)}(0)$ is chosen as $\text{Max}(f) - \text{Min}(f)/\pi = 35.33$. The coordinate $[-\overline{c}^{(0)}(2),\, -\overline{c}^{(0)}(3)]$ is the center of the elliptical contour and is here estimated to be $\overline{c}^{(0)}(2) = -39$ and $\overline{c}^{(0)}(3) = -42$. The initial value of coefficient $\overline{c}^{(0)}(4)$ is the squared value of either the major axis or minor axis of the elliptical contour depending on whether the coefficient $\overline{c}^{(0)}(5)$ is greater than or less than one. With *a priori* knowledge of the size range of cervical cells this coefficient can be set to the average value. In our experiment, $\overline{c}^{(0)}(4)$ is set to 400. The coefficient $\overline{c}^{(0)}(5)$ is the ratio of the two axes of the ellipse and is initially set to one corresponding to a circular contour as the initial approximation. With $\overline{c}^{(0)}(5)$ set to 1, the coefficient $\overline{c}^{(0)}(6)$, reflecting the orientation of the elliptical contour, can be set to zero as its initial value. The initial image $\hat{f}_{\overline{\mathbf{c}}^{(0)}}(n_1,\,n_2)$ corresponding to the initial vector given above and constant $A = 1$ is displayed in Fig. 1(b).

The algorithm searches for a better fit to the cell image by adjusting the parameters $\overline{c}^{(0)}(i)$, for $i = 0,\,1,\,\cdots,\,6$. It consists of the coarse optimization followed by the fine optimization procedures. In the coarse optimization procedure, $2L + 1$ samples are taken for each coefficient about the initial value specified above and the sampling period for the ith coefficient is Δ_i. The search range for each coefficient

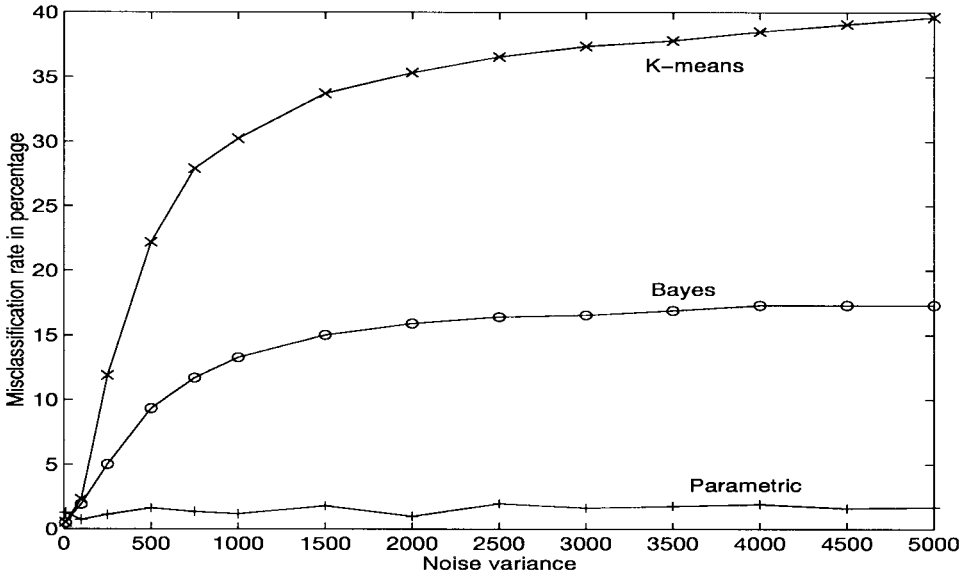

(a)

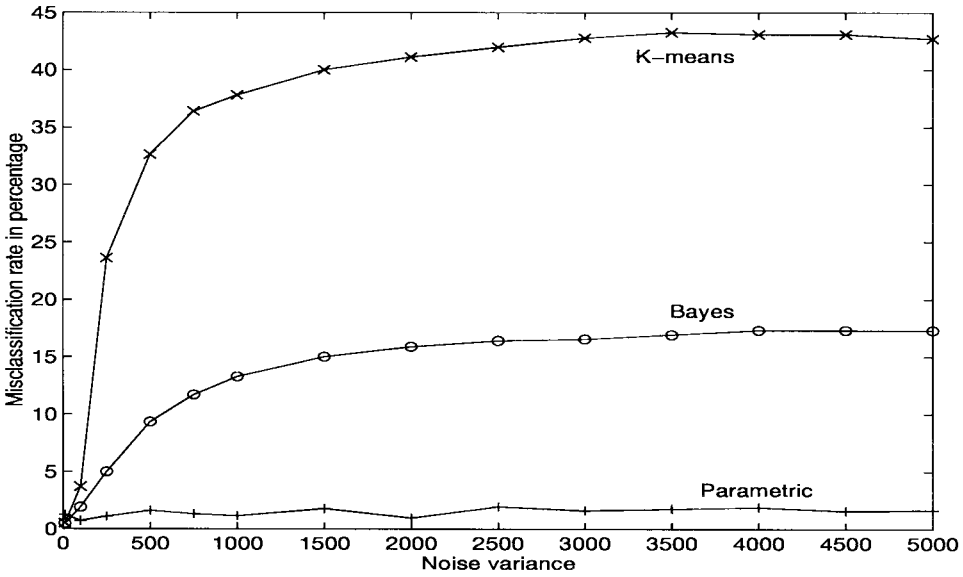

(b)

Fig. 2. Comparison of misclassification rate of the parametric fitting approach to a Bayes classifier and the two-level K-means clustering method on the distorted images blurred by a cylinder impulse response of radius $r_{mv} = 2.5$ and independent white Gaussian noise of variant levels. (a) Circular radius of 15 pixels and (b) circular radius of ten pixels.

is limited by the dynamic range of the coefficient which is determined from the *a priori* knowledge, such as $0 < c_0 < 255$, $0 < c_1 < 255$, $-N_1 < c_2 < 0$, $-N_2 < c_3 < 0$, $0 < c_4$, $0 < c_5$, and $-\pi < c_6 \leq \pi$. The actual search range is generally much smaller than the dynamic range so reducing the sampling period maintains the original number of samples for computation. In our experiments the sampling periods are selected as $\Delta_0 = \Delta_1 = 50/L$, $\Delta_2 = \Delta_3 = 10/L$, $\Delta_4 = 100/L$, $\Delta_5 = 0.9/L$, and $\Delta_6 = (\pi/2L)$, and $L = 100$. Smaller L makes the coarse search quicker, however, may result in a slower subsequent fine optimization when the coarse search provides a less accurate solution. The termination threshold δ for the coarse search procedure is set to be 0.000 01. The termination criterion for the iterative fine optimization procedure is that the magnitude of adjustment $\|\eta\Delta\mathbf{c}^{(k)}\| < 0.001$. The adjustment constant η should be selected as small as possible since large values may cause an already very closed solution to the global optima to turn away from it. We have tested different values for η on the image in Fig. 1(a) and found that when $\eta \leq 0.0002$ the fine optimization procedure converges. We set η to be 0.000 05 in our experiments. The final parameter vector estimated is $\mathbf{c} = (18.83\,96.2\,-40.1\,-46.2\,321\,0.44\,-0.129)^t$. The corresponding fitting function is shown in Fig. 1(c). The cell region is determined based on the fitting function in Fig. 1(c) by a thresholding process such as $\{(n_1, n_2) | \hat{f}_{\mathbf{c}}(n_1, n_2) \leq c_4\}$. To visually evaluate the match the original cell image with the extracted cell contour superimposed is shown in Fig. 1(d). For visual comparison Fig. 1(e) displays the segmentation with the two-class K-means clustering method [9] which iteratively updates the representative cluster centroids using the minimum means-square-distortion criteria. It is observed that in Fig. 1(d) the contour from the parametric fitting approach is rather smooth and matches the cell very well, while the K-means algorithm shown in Fig. 1(e) displays a noisy extracted cell contour and large misclassification regions.

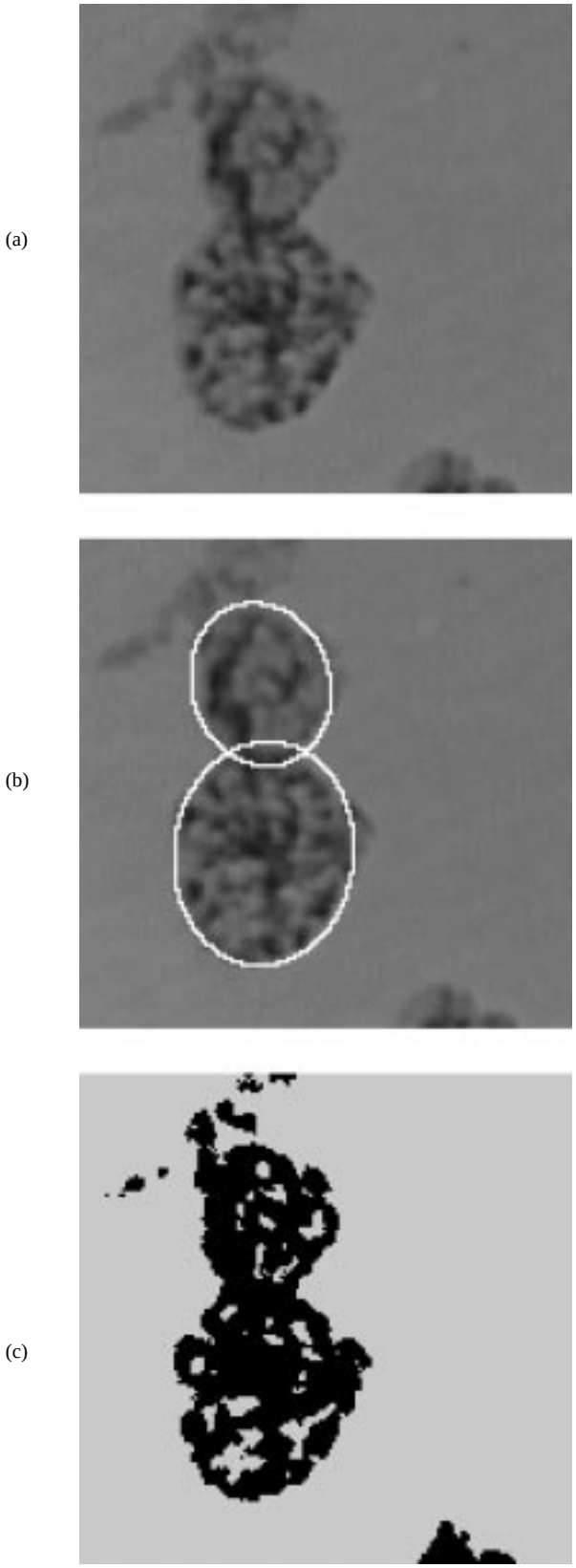

Fig. 3. Segmentation of overlapped breast cell image. (a) Original breast cell image, (b) extracted elliptical cell regions by the proposed algorithm, and (c) classification by the K-means clustering method.

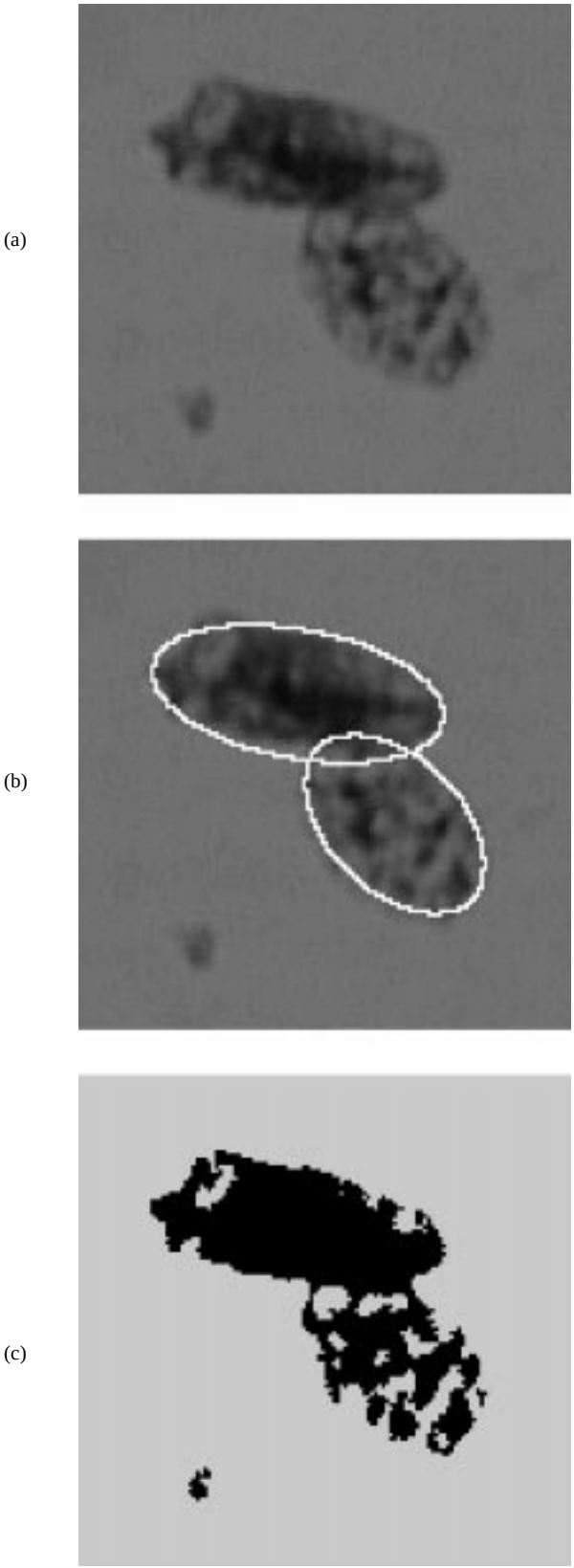

Fig. 4. Segmentation of another overlapped breast cell image. (a) Original breast cell image, (b) extracted elliptical cell regions by the proposed algorithm, and (c) classification by the K-means clustering method.

A synthetic cell image with known segmentation was used to quantitatively compare the proposed algorithm to a Bayes classifier and the K-means clustering algorithm. Let the synthetic cell image, size of 64×64, be a corrupted two-level image whose intensities are

TABLE I
PROCESSING TIME

	Fig.1	Fig. 3	Fig. 4
Running time	3'50.73"	3'52.73"	52'33.9"

100 inside a circular cell of radius r and 150 outside. The corruption includes blurring by a moving average filter with cylindrical impulse response of radius of r_{mv} plus additive independent white Gaussian noise of zero mean and variance σ_n^2. Discrimination of the cell region is made difficult by the blurring system and the additive image noise and results in misclassified pixels throughout the image. Fig. 2(a) and (b) shows the error rates in percentage for the parametric approach, a Bayes classifier as well as the K-means clustering method for the synthetic cell image with r being 15 and 10, respectively, as $r_{mv} = 2.5$ and σ_n^2 varied between 10 and 5000. It is observed that both a Bayes classifier and the K-means method perform well on images with low noise but poor with high noise. The classification error quickly increases monotonically with increasing noise. The parametric approach, however, is very robust to image noise and the misclassification rate remains low as the large noise range tested. Inspection of the processed images show that the errors of a Bayes classifier and the K-means clustering method appear throughout the image domain. In comparison, the errors of the parametric algorithm appear only at the cell boundaries.

Figs. 3 and 4 provide the image segmentation results of overlapped breast cells. Figs. 3(a) and 4(a) are the original images of overlapped breast cells which are highly textured. Figs. 3(b) and 4(b) show the segmentations of the proposed algorithm. In the algorithm, segmentation of two overlapped cells is obtained by determining the two sets of coefficients $\overline{c}_i$ and $\overline{c}'_i$, for $i = 2, 3, \cdots, 6$, respectively. The initial coefficients, $\overline{c}_i^{(0)}$, for $i = 0, 1, \cdots, 6$, were selected in the same manner as when processing an isolated cell in the coarse search. The initial parameters of the second cell, $\overline{c}_i'^{(0)}$, for $i = 4, 5, 6$, were selected identical to those of the first cell, i.e., $\overline{c}_i'^{(0)} = \overline{c}_i^{(0)}$, for $i = 4, 5, 6$. Since the two cell centers are separated by some distance we have $\sqrt{[\overline{c}_2'^{(0)} - \overline{c}_2^{(0)}]^2 + [\overline{c}_3'^{(0)} - \overline{c}_3^{(0)}]^2} \geq \gamma$, where γ is a constant approximating the distance between the two ellipse centers. The initial coefficients $\overline{c}_2'^{(0)}$ and $\overline{c}_3'^{(0)}$ were set to the coordinate where the smoothed original cell image is minimum and located a distance greater than γ from the previously estimated center of the first cell. Since cytological cells are usually not severely overlapped, we can specify the value of γ to be about half the minor axis of the smallest cell. In our experiments we selected γ to be 50. The segmentation is not sensitive to the value of γ; values for γ between 30 and 70 produced almost the identical segmentations for both images. Compared to the K-means clustering method, shown in Figs. 3(c) and 4(c), the proposed algorithm produces much better results based on visual evaluation. The extracted cell contours by the proposed algorithm match the cell regions very well while the K-means clustering method results in substantial misclassification and can not separate the overlapped cell contours.

We have run our program in C code on a Sun Sparc 20 platform. The consumed time for the experiments is listed in Table I, we observe that the processing of the overlapped cells is computationally very extensive while processing of the isolated cells consumes much less time.

VII. CONCLUSIONS

We introduced a parametric elliptical fitting algorithm for segmentation of elliptically shaped cells in light microscopy images. Experiments were performed on cervical and breast cells that have approximately elliptical shapes. Cervical cell images usually have noisy background corrupted by small artifact spots, while breast cells are highly textured. The proposed algorithm is successful largely because it employs both the shape information and the regional image information. Incorporating the shape information significantly reduces the number of parameters and thus reduces the freedom of the cell contour. Unlike the Hough transform that uses the edge information, the fitting of the parametric image to the original incorporates image information of not only the edge but also the interiors and exteriors of cells. Experimental results for synthetic images show the proposed algorithm greatly outperforms the Bayes classifier and the K-means clustering method. Results on real noisy cervical cell and textured breast cell images are also provided. Visual evaluation and comparison with the two-level K-means algorithm demonstrate the superior performance of the proposed algorithm. The computation of the algorithm is rather complicated especially for those overlapped cell images.

REFERENCES

[1] J. Gil and J. Barba, "Morphometry in image analysis for anatomic pathology," in *Image Analysis: A Primer for Pathologists,* A. M. Marchevsky and P. H. Bartels, Eds. Raven, NY: 1994, pp. 79–124.

[2] J. P. A. Baak, *Manual of Quantitative Pathology in Cancer Diagnosis and Prognosis.* NY: Springer-Verlag, 1991.

[3] P. W. Hamilton and D. C. Allen, Eds., *Quantitative Clinical Pathology.* Oxford, U.K. : Blackwell, 1995.

[4] A. J. Einstein, J. Barba, P. D. Unger, and J. Gil, "Nuclear diffuseness as a measure of texture: Definition and application to the computer-assisted diagnosis of parathyroid adenoma and carcinoma," *J. Microscopy,* vol. 176, pt. 2, pp. 158–166, Nov. 1994.

[5] H.-S. Wu and J. Barba, "An efficient semi-automatic algorithm for cell contour extraction," *J. Microscopy,* vol. 179, pt. 3, pp. 270–276, Sept. 1995.

[6] J. Canny, "Computational approach to edge detection," *IEEE Trans. Pattern Anal. Machine Intell.,* vol. PAMI-8, pp. 679–698, 1986.

[7] S. Sarkar and K. Boyer, "On optimal infinite impulse response edge detection filters," *IEEE Trans. Pattern Analys. Machine Intell.,* vol. 13, Nov. 1991.

[8] Y.-H. Kim and S. D. Kim, "Image flow segmentation and estimation using displaced spatial gradient," *Inst. Electr. Eng. Electronics Lett.,* vol. 28, pp. 2213–2215, 1992.

[9] J. T. Tou and R. C. Gonzalez, *Pattern Recognition Principles.* Reading, MA: Addison-Wesley, 1982.

[10] W.-N. Lie, "Automatic target segmentation by locally adaptive image thresholding," *IEEE Trans. Image Process.,* vol. 4, pp. 1036–1041, July 1995.

[11] M. A. Wani and B. G. Batchelor, "Edge-region-based segmentation of range images," *IEEE Trans. Pattern Analys. Machine Intell.,* vol. 16, pp. 314–319, Mar. 1994.

[12] H.-S. Wu and J. Barba, "An algorithm for noisy cell contour extraction via area merging," *J. Imag. Sci., Technol.,* vol. 38, pp. 604–607, Nov. 1994.

[13] R. Adams and L. Bischof, "Seeded region growing," *IEEE Trans. Pattern Analys. Machine Intell.,* vol. 16, pp. 641–647, June 1994.

[14] C. Garbay, "Image structure representation and processing: A discussion of some segmentation methods in cytology," *IEEE Trans. Pattern Anal. Machine Intell.,* vol. PAMI-8, pp. 140–146, Mar. 1986.

[15] S. S. Trivedi, G. T. Herman, and J. K. Udupa, "Segmentation into three classes using gradients," *IEEE Trans. Med. Imag.,* vol. MI-5, pp. 116–119, Jun. 1986.

[16] K. S. Fu, *Digital Pattern Recognition.* New York: Springer-Verlag, 1980.

[17] K. Fukunaga, *Introduction to Statistical Pattern Recognition.* New York: Academic, 1979.

[18] V. F. Leavers, "The dynamic generalized Hough transform: Its relationship to the probabilistic Hough transforms and an application to the concurrent detection of circles and ellipses," *CVGIP: Image Understanding,* vol. 56, pp. 381–398, Nov. 1992.

[19] P.-K. Ser and W.-C. Siu, "Novel detection of conics using 2-D Hough planes," *IEEE Proc. Vision, Image Signal Processing,* vol. 142, pp. 262–270, Oct. 1995.